Supplemental Material for

Robust Ellipsoid-specific Fitting via Expectation Maximization

Mingyang Zhao
zhaomingyang16@mails.ucas.ac.cn
Beijing Academy of Artificial Intelligence (BAAI) and NLPR, Institute of Automation, CAS, Beijing, China
Xiaohong Jia†
xhjia@amss.ac.cn
Academy of Mathematics and Systems Science, CAS, Beijing, China
Lei Ma†
lei.ma@pku.edu.cn
National Engineering Laboratory for Video Technology, Peking University, and BAAI, Beijing, China
Xinlin Qiu
qiuxinling@hbc.edu.cn
College of Artificial Intelligence, Hubei Business College, Wuhan, Hubei
Xin Jiang
jiangxin@buaa.edu.cn
School of Mathematical Science, Beihang University, Beijing, China
Dong-Ming Yan
yandongming@gmail.com
NLPR, Institute of Automation, CAS and the University of CAS, Beijing, China
† Corresponding author

In this document, we provide additional details, discussions, and experiments to support the original paper. Below is a summary of the contents:

- Derivation of the orthogonal point-to-ellipsoid distance for completeness;
- Derivation of the expectation of the complete-data negative log-likelihood function (Q function) of the EM algorithm;
- Derivation of the geometric parameters of an ellipsoid;
- Parameter settings of other compared methods in the paper;
- Application of the proposed method for shape approximation;
- Generalization of the proposed method for other quadric fitting.

1 Derivation of the Orthogonal Point-to-Ellipsoid Distance

We present a simple derivation here of the orthogonal distance from a point to an ellipsoid to show its computational complexity. Let the equation of the ellipsoid $\mathcal{E}(x,y,z)$ with center (x_o,y_o,z_o) be

$$A(x-x_o)^2+B(y-y_o)^2+C(z-z_o)^2+D(x-x_o)(y-y_o)+E(x-x_o)(z-z_o)+F(y-y_o)(z-z_o)-1=0. \tag{1}$$

Given a point $\mathbf{x}=(x,y,z)$ not lying on the ellipsoid and suppose its closet point on the ellipsoid is $\mathbf{x}_t=(x_t,y_t,z_t)$, then we have

$$\mathcal{E}(x_t,y_t,z_t)=0. \tag{2}$$

Since the tangent at $\mathbf{x}_t$ is orthogonal to the vector $\mathbf{x}-\mathbf{x}_t$, thereby

$$(x-x_t)*\frac{\partial}{\partial y}\mathcal{E}(x_t,y_t,z_t)=(y-y_t)*\frac{\partial}{\partial x}\mathcal{E}(x_t,y_t,z_t). \tag{3}$$

Let $\Delta x = x_t - x_o$, $\Delta y = y_t - y_o$, and $\Delta z = z_t - z_o$, from Eq. 1, we have

$$A\Delta^2 x+B\Delta^2 y+C\Delta^2 z+D\Delta x\Delta y+E\Delta x\Delta z+F\Delta y\Delta z-1=0.$$

Then we get

$$\Delta y=\frac{-(D\Delta x+F\Delta z)+\eta_1}{2B}, \Delta z=\frac{-(E\Delta x+F\Delta y)+\eta_2}{2C}, \tag{4}$$

where

$$\eta_1^2=(D\Delta x+F\Delta z)^2-4B(A\Delta^2 x+C\Delta^2 z+E\Delta x\Delta z-1), \tag{5}$$
$$\eta_2^2=(E\Delta x+F\Delta y)^2-4C(A\Delta^2 x+B\Delta^2 z+D\Delta x\Delta y-1). \tag{6}$$

From Eq. 3 we get

$$(x-x_0-\Delta x)(2B\Delta y+D\Delta x+F\Delta z)=(y-y_0-\Delta y)\cdot(2A\Delta x+D\Delta y+E\Delta z). \tag{7}$$

Substituting Δy into the above equation and squaring the result leads to the following equation:

$$4B^2(x-x_0-\Delta x)^2\eta_1^2=(2B(y-y_0)+\Delta x+F\Delta z-\eta_1)^2\cdot(2A\Delta x+D\Delta y+E\Delta z)^2. \tag{8}$$

Combining Δz in Eq. 4 and η_1^2 in Eq. 5, we know that the above equation is sixth order in terms of Δx, thereby, we require solving a sixth order equation to attain $(\Delta x, \Delta y, \Delta z)$, and then the orthogonal distance d is computed by

$$d=\sqrt{(x-x_o-\Delta x)^2+(y-y_o-\Delta y)^2+(z-z_o-\Delta z)^2}.$$

From the above derivation, we know that it is difficult to directly take the exact orthogonal distance into the geometric fitting.

2 Q Function

In the M-step of EM framework, the "new" parameter Ω is updated by minimizing the expectation of the complete-data negative log-likelihood function (Q function), namely

$$\begin{aligned} Q(\Omega,\Omega^{old}) &= \mathbf{E}_{\mathbf{Y}}[-\log p(\mathbf{Y},\mathbf{X}|\Omega)|\mathbf{X},\Omega^{old}] \\ &= -\Sigma_{\mathbf{Y}}\log p(\mathbf{Y},\mathbf{X}|\Omega)p(\mathbf{Y}|\mathbf{X},\Omega^{old}) \\ &= -\Sigma_{i=1}^{N}\Sigma_{m=1}^{M+1}p^{old}(\mathbf{y}_m|\mathbf{x}_n)\log(p^{new}(\mathbf{y}_m)p^{new}(\mathbf{x}_i|\mathbf{y}_m)) \\ &= \frac{1}{2\sigma^2}\Sigma_{i=1}^{N}\Sigma_{m=1}^{M}p^{old}(\mathbf{y}_m|\mathbf{x}_i,\Omega)\|\mathbf{x}_i-(\mathbf{A}\mathbf{y}_m+\mathbf{t})\|^2 \\ &+\frac{N_p d}{2}\log\sigma^2-\log(w)N_o-\log(1-w)N_p, \end{aligned} \tag{9}$$

where $p(\mathbf{x},\mathbf{y}_{m+1})=\frac{w}{V}$ represents the point $\mathbf{x}$ sampled from the uniform distribution $\frac{1}{V}$, $N_o = \sum_{i=1}^{N}p^{old}(\mathbf{y}_{m+1}|\mathbf{x}_i,\Omega)$, and $N_p=\sum_{i=1}^{N}\sum_{m=1}^{M}p^{old}(\mathbf{y}_m|\mathbf{x}_n,\Omega)$. Note that we have ignored the independent term of Ω in Eq. 9.

3 Ellipsoid Parameter

To get ellipsoid parameters, we reformulate the second-order polynomial of an ellipsoid as follows.

Definition 1 *An ellipsoid surface $e \in \mathbb{R}^d$ in center form can be represented by*

$$e = \{\mathbf{x} \in \mathbb{R}^d | (\mathbf{x} - \mathbf{c}_e)^T \mathbf{B}^{-1} (\mathbf{x} - \mathbf{c}_e) = 1\}, \tag{10}$$

where $\mathbf{c}_e \in \mathbb{R}^d$ is the ellipsoid center and $\mathbf{B} \in \mathbb{S}^d_{++}$ is the shape matrix.

Since the unit sphere (attained in paper) with center $\mathbf{c}_s$ is $(\mathbf{y}_m - \mathbf{c}_s)^T(\mathbf{y}_m - \mathbf{c}_s) = 1$, then the fitted ellipsoid is

$$[\mathbf{x} - (\hat{\mathbf{t}} + \hat{\mathbf{A}}\mathbf{c}_s)]^T (\hat{\mathbf{A}}\hat{\mathbf{A}}^T)^{-1} [\mathbf{x} - (\hat{\mathbf{t}} + \hat{\mathbf{A}}\mathbf{c}_s)] = 1, \tag{11}$$

thereby $\hat{\mathbf{B}} = \hat{\mathbf{A}}\hat{\mathbf{A}}^T$ and $\hat{\mathbf{c}_e} = \hat{\mathbf{t}} + \hat{\mathbf{A}}\mathbf{c}_s$ are the shape matrix and the center of the result ellipsoid. By eigenvalue decomposition, we have $\hat{\mathbf{B}} = \mathbf{Q}^T \Lambda \mathbf{Q}$, where $\mathbf{Q}_{3\times3}$ and $\Lambda_{3\times3}$ are the rotation and the diagonal matrix, respectively, with eigenvalues equal to λ_1, λ_2, and λ_3. Finally, the nine geometric parameters of an ellipsoid are

$$\boxed{\begin{array}{llll} \hat{\mathbf{c}}_e = \hat{\mathbf{t}} + \hat{\mathbf{A}}\mathbf{c}_s, & \hat{a} = \sqrt{\lambda_1}, & \hat{b} = \sqrt{\lambda_2}, & \hat{c} = \sqrt{\lambda_3}, \\ \hat{\alpha} = \operatorname{atan2}\dfrac{-\mathbf{Q}_{31}}{\sqrt{(\mathbf{Q}_{11} + \mathbf{Q}_{21})^2}}, & \hat{\beta} = \operatorname{atan2}\dfrac{\mathbf{Q}_{21}}{\mathbf{Q}_{11}}, & \hat{\gamma} = \operatorname{atan2}\dfrac{\mathbf{Q}_{32}}{\mathbf{Q}_{33}}. & \end{array}} \tag{12}$$

4 Implementation Details

We manually tune the hyper-parameters of compared methods to achieve their best performance, as listed below:

- MQF: We reimplement MQF according to the pseudo code of [1], as faithfully as possible. In reimplementation, we adopt the local plane fitting for normal estimation, where nine closet neighborhood points are sampled. To accommodate noise and outlier interference, the weight value (hyper-parameter) is set as 0.3, by which the gradient-normal alignment effect is depressed.

- RIX: The maximal step size in the iteration of RIX is tuned from 50 to 100, whereas the minimal one is set as 0.001. The scale factor of RIX is tuned for each test such as 1.5 and 6, since fixed value often leads to noticeable deviations.

Note that our proposed method need not manually tune parameters, and all parameters are updated automatically.

5 More Examples

We provide more fitting examples to further demonstrate applications of the proposed method.

(1) **3D magnetometer calibration.** Ellipsoid fitting plays a dominate role for magnetometer calibration, by which the accurate direction and strength of magnetism can be measured. For instance, compass as a kind of magnetometer tells us the orientation via the

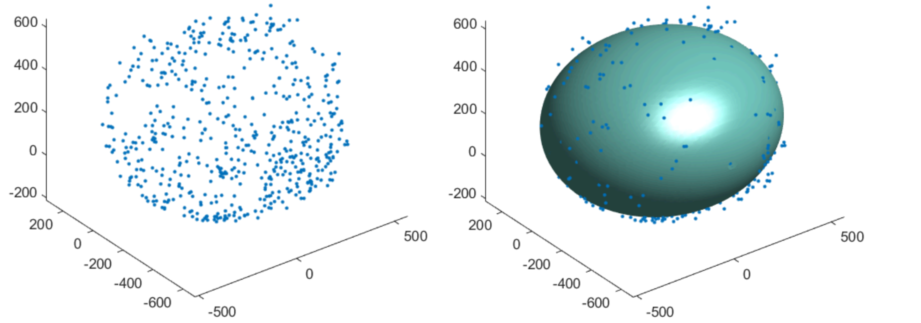

Figure 1: Application of the proposed method for 3D magnetometer calibration, by which the direction and strength of magnetism is measured.

measuring of the earth's magnetic field. Fig. 1 exhibits several real magnetometer data [1] and the fitting result by the proposed method. Although the interference of heavy noise and point heterogeneity, the ellipsoid still provides a fairly exact estimation, thereby the offset can be effectively eliminated after the calibration.

(2) **Shape approximation.** As shown in Fig. 2, for the triangle mesh data, *ie*., "bun 000"[2], "Max Planck bust" [3], "cow"[4], and "pear"[5], we down sample vertices and then directly input them to our algorithm. As observed, apart from the major part (the part need ellipsoid fitting), there has plentiful interference (other parts). For instance, the body of bunny is the main part for fitting, whereas its head and ears are outliers. However, our method is greatly robust against outliers, and shows sound approximation for the corresponding part. For two ellipsoid cases, we conduct a simple segmentation after the first fitting. Results indicate that the proposed method is competent in providing highly accurate approximation.

6 Generalized Geometric Primitive Fitting

Actually, the proposed method can be directly customized for other geometric primitive fitting. To test this, we randomly generate several point clouds of cylinders, cones and degenerate planes, which are contaminated by heavy noise and outliers, as illustrated in Fig. 3. As observed, our algorithm still attains successful fits for all cases. Thereby, replacing the parametric form of ellipsoids by other quadrics, our proposed framework can be extended to fit general primitives, especially in the presence of outliers.

[1] https://github.com/risherlock/Magnetometer-Calibration
[2] http://graphics.stanford.edu/data/3Dscanrep/
[3] https://www.mpg.de/institutes
[4] https://gfx.cs.princeton.edu/proj/sugcon/models/
[5] https://gfx.cs.princeton.edu/pubs/Kalnins_2002_WND/index.php

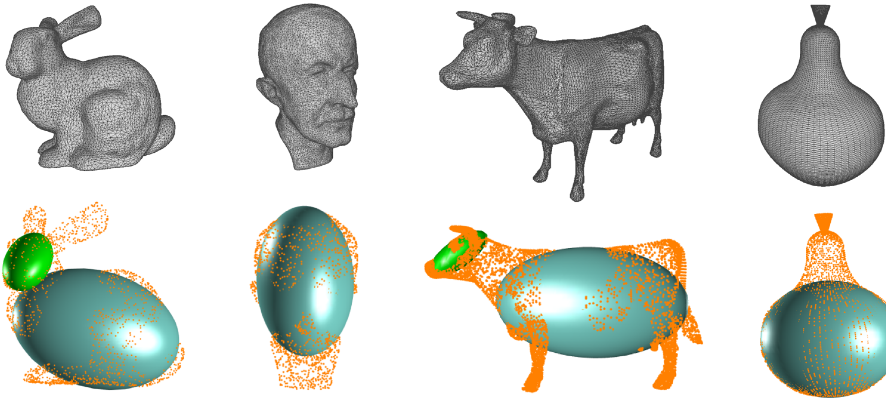

Figure 2: Application of the proposed method for shape approximation. Although the interference of other parts (outliers), our method still successfully fits the major parts for all cases.

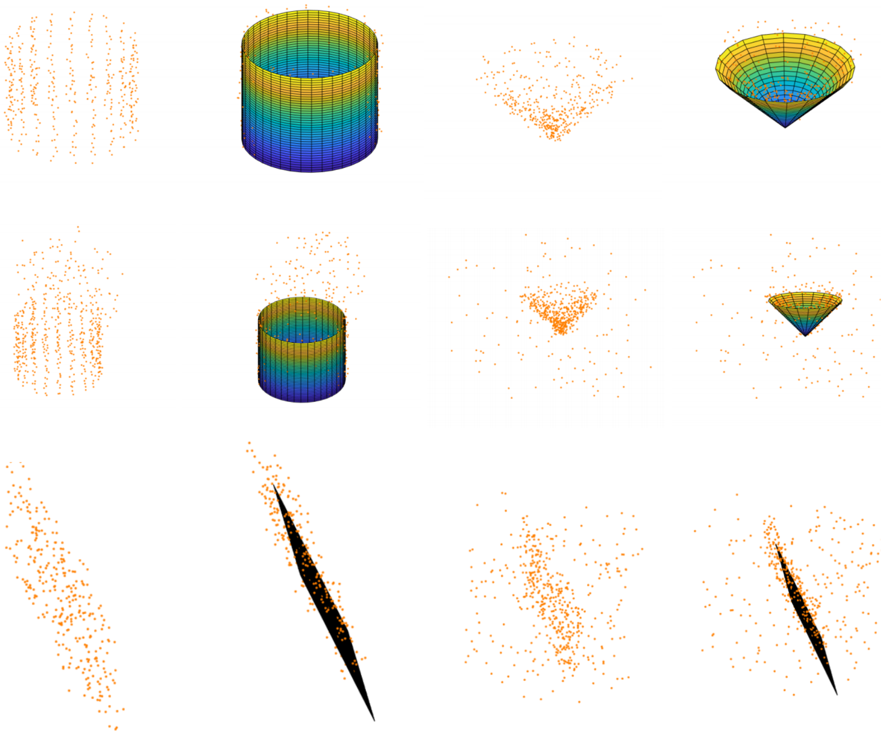

Figure 3: Generalizing the proposed method for other geometric primitive fitting under the contamination of noise and outliers, as observed, our method still attains promising results.

References

[1] Tolga Birdal, Benjamin Busam, Nassir Navab, Slobodan Ilic, and Peter Sturm. Generic primitive detection in point clouds using novel minimal quadric fits. *IEEE Transactions*

on Pattern Analysis and Machine Intelligence, 42(6):1333–1347, 2019.

[2] Richard I Hartley. In defense of the eight-point algorithm. *IEEE Transactions on Pattern Analysis and Machine Intelligence*, 19(6):580–593, 1997.